Near-infrared diffuse correlation spectroscopy in cancer diagnosis and therapy monitoring

Guoqiang Yu

Near-infrared diffuse correlation spectroscopy in cancer diagnosis and therapy monitoring

Guoqiang Yu
University of Kentucky, Center for Biomedical Engineering, Lexington, Kentucky 40506-0070

Abstract. A novel near-infrared (NIR) diffuse correlation spectroscopy (DCS) for tumor blood flow measurement is introduced in this review paper. DCS measures speckle fluctuations of NIR diffuse light in tissue, which are sensitive to the motions of red blood cells. DCS offers several attractive new features for tumor blood flow measurement such as noninvasiveness, portability, high temporal resolution, and relatively large penetration depth. DCS technology has been utilized for continuous measurement of tumor blood flow before, during, and after cancer therapies. In those pilot investigations, DCS hemodynamic measurements add important new variables into the mix for differentiation of benign from malignant tumors and for prediction of treatment outcomes. It is envisaged that with more clinical applications in large patient populations, DCS might emerge as an important method of choice for bedside management of cancer therapy, and it will certainly provide important new information about cancer physiology that may be of use in diagnosis. © *2012 Society of Photo-Optical Instrumentation Engineers (SPIE)*. [DOI: 10.1117/1.JBO.17.1.010901]

Keywords: diffusion; correlation; spectroscopy; blood flow; cancer; therapy.

Paper 11425V received Aug. 4, 2011; revised manuscript received Nov. 8, 2011; accepted for publication Nov. 14, 2011; published online Feb. 7, 2012.

1 Introduction

Early cancer detection can dramatically improve treatment outcomes. For example, finding breast cancers when they remain localized results in 5-year survival rates of 90% or higher.[1] Abnormal tissue hemodynamics and metabolism in tumor may precede detectable morphological changes of tumor, thus providing early diagnostic information.[2] High concentrations of hemoglobin with low oxygen saturation are suggestive of tumors, due to their high metabolic demand and/or (sometimes) poor perfusion. Also, measurement of tumor hemodynamic changes during cancer treatment is particularly attractive for cancer therapies that require tissue oxygen for treatment efficacy. Patients with hypoxic tumors are well known to show only minimal improvements in response to radiation and photodynamic therapies.[3–5] Moreover, cancer therapy can alter tumor hemodynamic and metabolic status, which impacts further treatment outcomes.[2,5] Expectations are that functional assessment of tumor hemodynamics and metabolism before, during and after cancer therapy in each patient provides information for the early prediction and longitudinal evaluation of therapeutic outcomes, thus enabling clinicians to make treatment decisions and optimize individual treatment.

Tumor hemodynamics and metabolism, however, are not routinely measured during cancer therapy due to the lack of appropriate technologies. Current diagnostic tools for cancers include ionizing or nonionizing radiological techniques such as X-ray mammography, computed tomography (CT), positron emission tomography (PET), functional magnetic resonance imaging (fMRI) and ultrasound imaging.[6] Some of these techniques primarily provide morphological information about tumors (e.g., CT, ultrasound), and others (e.g., PET, fMRI) provide functional information. However, a positive test usually requires further examination of the tissue with biopsy. Furthermore, although some of these imaging techniques have improved tremendously during recent decades (e.g., CT, PET, fMRI), they are relatively expensive low-throughput technologies which can involve exposure to ionizing radiation (e.g., CT, PET), and thus their frequent application is limited.

Near-infrared spectroscopy (NIRS) has recently attracted attention as a simple, fast, portable, noninvasive and inexpensive method for functional diagnosis and therapeutic monitoring of cancer diseases.[2] A well-known spectral window exists in the near-infrared (NIR) range (650 to 950 nm) wherein tissue absorption is relatively low so that light can penetrate into deep/thick volumes of tissue (up to several centimeters). NIRS provides a fast and portable alternative to costly imaging techniques (e.g., fMRI, PET, CT) for measurement of tissue optical properties at the level of microvasculature, although it has relatively poor spatial resolution when probing deep tissues: ~0.5 mm near the surface and the resolution degrades with depth. Endogenous tumor-to-normal contrasts available to NIRS include: tissue absorption; scattering; concentrations of oxy-, deoxy-, and total-hemoglobin, water and lipids; and blood oxygen saturation.[7–15]

A relatively new *dynamic* NIR technique, namely diffuse correlation spectroscopy (DCS)[16,17] or diffuse wave spectroscopy (DWS),[18–20] has been developed which can directly measure the motions of red blood cells in biological tissues while also maintaining all the advantages of NIRS. DCS flow measurements are accomplished by monitoring speckle fluctuations of photons induced by the moving scatterers in tissues. In nonmuscular tissues moving red blood cells (RBCs) inside vessels are primarily responsible for these fluctuations, but complications such as fiber shearing and motion artifacts can arise, especially

Address all correspondence to: Guoqiang Yu, University of Kentucky, Center for Biomedical Engineering, Lexington, Kentucky 40506-0070. Tel: 8592579110; E-mail: guoqiang.yu@uky.edu.

in muscular tissues.[21,22] DCS provides several new attractive features for blood flow measurement in microvasculature, such as noninvasiveness, portability,[23] high temporal resolution (up to 100 Hz),[24] and relatively large penetration depth (up to several centimeters).[25–27] DCS can be easily and continually applied at the bedside in clinical rooms.[28–34] DCS measurements of blood flow variations in biological tissues have been compared against other standards, including power Doppler ultrasound,[5,35] laser Doppler,[36] Xenon-CT,[37] Doppler ultrasound,[34,38] fluorescent microsphere flow measurement,[39] histology and nitroimidazole hypoxia markers (EF5),[29] and perfusion MRI.[27,40] These validation studies have shown that DCS flow measurements are in good agreement with other flow measurement techniques.

The utility of DCS technology for monitoring of deep tissue blood flow has been demonstrated in brain,[20,27,32–34,37–39,41–49] muscle,[22,23,26,31,36,40,50] and tumor.[5,21,25,28,30,35,51–57] DCS was first applied to tumor study in 2003[35] and has been used less in the "cancer" context than in other scenarios such as brain and muscle. Therefore, a review of potential for cancer applications of DCS is valuable at this time for both optical and cancer communities. This review is not intended to discuss every detail about DCS; rather it provides a flavor for the DCS method and a snapshot of its recent progress in cancer research. For example, DCS has been utilized in the monitoring of tumor-to-normal flow contrasts[25,30] and early hemodynamic/metabolic responses to chemotherapy[30] in human breast cancers, physiological effects of chemoradiation therapy on human head and neck cancers,[29,53] hemodynamic responses to photodynamic therapy (PDT) in human prostate cancers,[28,51] and efficacies of PDT in murine tumor models.[5,35,55–57] In some of these studies, DCS was combined with NIRS in hybrid instruments for accurately extracting tumor blood flow[21] and for calculating tumor metabolic rate of oxygen consumption (TMRO$_2$) from the measured flow and oxygenation data.[30] It is expected that measurements with multiple hemodynamic and metabolic parameters have the potential to enhance sensitivity and specificity in detection of cancers and monitoring of therapies.

The review first outlines the basic principle and instrumentation of DCS. It then focuses on introducing application examples of DCS in cancer diagnosis and treatment monitoring. Interested readers are encouraged to consult primary references for more details. Finally, it summarizes the advantage of DCS technique and the limitation of current studies using DCS, and points out future perspectives.

2 Diffuse Correlation Spectroscopy

When using NIRS to noninvasively detect optical properties of deep tissues, a pair of source and detector fibers is usually placed along the tissue surface with a distance of a few centimeters. NIR light generated by a laser emits into tissues through the source fiber and is detected by a photodetector through the detector fiber. Photon migration in tissue is known to behave as a diffusive process and can be characterized using the photon diffusion equation.[7–13] During this migration, photons experience absorption and scattering events. The probabilities for the occurrence of these events are described by absorption and scattering coefficients. The difference in NIR absorption spectra between major tissue chromophores allows for the measurement of oxygenated and deoxygenated hemoglobin concentrations, total hemoglobin concentration, and blood oxygen saturation. The penetration depth of NIR light in biological tissues is approximately half of the source-detector distance along the tissue surface.

The dynamic or correlation method (DCS) detects the motions of scatterers, typically starting with a similar measurement configuration as NIRS but employing coherent laser sources and single photon counting detectors. The temporal statistics (or frequency-domain analogs of temporal statistics) of the speckle fluctuations of the scattered light are measured, and the electric field temporal autocorrelation function or its Fourier transform is calculated from the measured light intensity autocorrelation function. Using a correlation diffusion equation describing the propagation of the electric field temporal autocorrelation function through tissues,[16,17,58] the measured signal can then be related to the motion of scatterers. In the case of tissues, the primary moving scatterers are RBCs. Consequently, blood flow can be determined.

Figure 1(a) shows a typical portable DCS system.[23] A long coherence length (>5 m) laser light source (e.g., IRCL-100-785-S, Crystalaser.com, CA) must be employed. Output from the laser can be delivered to the tissue through a multimode optical fiber. Single-mode[23] (or few-mode[20,49]) fibers should be used to collect photons from a single (or a few) speckle(s) emitted from the tissue surface. Fast photon-counting avalanche photodiodes (APDs) (e.g., SPCM-AQR-12, Perkin Elmer, CA) are generally used as detectors. A multitau correlator board (Correlator.com, NJ) takes the transistor-transistor-logic (TTL) outputs from the APDs and calculates temporal intensity autocorrelation functions of the detected light. The optical and electronic components are controlled through a computer.

The normalized light intensity temporal autocorrelation functions (g_2) measured from DCS is related to the normalized electric field temporal autocorrelation function (g_1) through the following Siegert relation,[59]

$$g_2(\overrightarrow{r}, \tau) = 1 + \beta|g_1(\overrightarrow{r}, \tau)|^2, \tag{1}$$

where τ is the correlation delay time, $\overrightarrow{r}$ is the position vector, and β depends on laser stability and coherence length and the number of speckles detected. Note, however, that the biological system studied must be assumed ergodic when applying the Siegert relation (see the discussion about this assumption in Section 5).[58]

Scatterer motion is directly associated with the unnormalized electric field temporal autocorrelation function (G_1) which obeys a correlation diffusion equation, derived rigorously elsewhere[58] and defined as follows for homogeneous media using a CW source (steady state):

$$\left(D\nabla^2 - v\mu_a - \frac{1}{3}v\mu_s'k_0^2\alpha\langle\Delta r^2(\tau)\rangle\right)G_1(\overrightarrow{r}, \tau) = -vS(\overrightarrow{r}), \tag{2}$$

where v is the speed of light in tissue, μ_a [cm^{-1}] is the tissue absorption coefficient, μ_s' [cm^{-1}] is the tissue reduced scattering coefficient, $D = v/(3\mu_s')$ is the photon diffusion coefficient, k_0 is the wavenumber, $S(\overrightarrow{r})$ is the source light distribution, and $\langle\Delta r^2(\tau)\rangle$ is the mean-square displacement of scatterers in delay time τ, which directly characterizes the scatterer movement. Since the scatterers in biological tissue

may be relatively static (e.g., nuclei, mitochondria) or dynamic (moving RBCs), a multiplicative factor, α (ranging from 0 to 1), is introduced to account for the fact that not all scatterers are "moving"; this factor is defined as the ratio of the total number of "moving" scatterers to the total number of scatterers. Again, the position vector, $\overrightarrow{r}$, denotes a general vector from the source to a point of detection.

RBCs pass through capillaries in single file and experience shear flow in larger vessels; the RBCs also experience tumbling motions in addition to translation. Intuitively, the random ballistic flow model might be considered the best model with which to fit DCS data. In practice, however, the diffusion model, i.e., $\langle \Delta r^2(\tau) \rangle = 6D_B\tau$, fits the autocorrelation curves rather well over a broad range of tissue types, ranging from rat brain,[43,45] and mouse tumor,[5,35] to piglet brain,[39] adult human skeletal muscle,[23,26] premature brain,[34,38] adult brain,[20,27,33,41] and adult tumors.[21,29,30] Here D_B is the effective Brownian diffusion coefficient. Therefore the combined term, αD_B, has been referred to as the blood flow index in biological tissues and has been commonly used to calculate relative blood flow (rBF) compared to the baseline flow index before physiological changes.

DCS can be used in many diverse situations requiring different probe designs. Figures 1(b)–1(d) show three example probes. The first probe (see Fig. 1(b)) with straight or 90-deg bent fibers is used in studies of tumors close to the body surface (e.g., breast tumor, head and neck tumor).[21,25,29,30] The second probe [see Fig. 1(c)] is a noncontact probe mounted on the imaging plane of a mechanical camera which is fixed at a certain distance (e.g., 15 cm) from the tumor surface.[5] This unique noncontact setup allows for a continuous monitoring of tumor hemodynamic changes during photodynamic therapy by permitting unobstructed illumination from treatment light. Finally, the third probe [see Fig. 1(d)] consists of multiple side-firing fibers embedded in a thin catheter which could be inserted into tissues/tumors with minimum tissue damage.[28] For different probe-tissue interfaces, different boundary conditions [e.g., semi-infinite geometry in Figs. 1(b) and 1(c) or infinite geometry in Fig. 1(d)] should be used to solve Eq. (2) for extracting blood flow index. Practically all innovations from the design of NIRS probes can be taken and adapted for DCS use, and hybrid probes for both NIRS and DCS can be easily built by adding extra source and detector fibers.[21,25,28–30]

3 Diagnostic Applications

DCS/NIRS has been previously tested for use in diagnosis of cancers where tumor blood flow, oxygenation, and oxygen metabolism (TMRO$_2$) were measured.[25,30] One such example is in the detection of tumor-to-normal flow contrast in breast tumors. In this case, two healthy subjects and five patients with palpable breast tumors were recruited.[25] These subjects were asked to lie supine flattening the breast, while experienced researchers scanned the tumor with a handheld optical probe [see Figs. 1(b) and 2(a)] in both horizontal and vertical directions in 1-cm increments across the tumor. Two scan directions allowed for checking the repeatability of the measurements. For healthy volunteers, an arbitrary region was drawn as the tumor site, and a measurement was obtained by scanning across that region. The control measurements provided information about the heterogeneity of blood flow in healthy breast tissues.

Figure 2 shows horizontal (b) and vertical (c) profiles from one malignant tumor and one healthy breast. There was only slight variation observable in the healthy breast; whereas, blood flow increased in both scan directions as the probe crossed
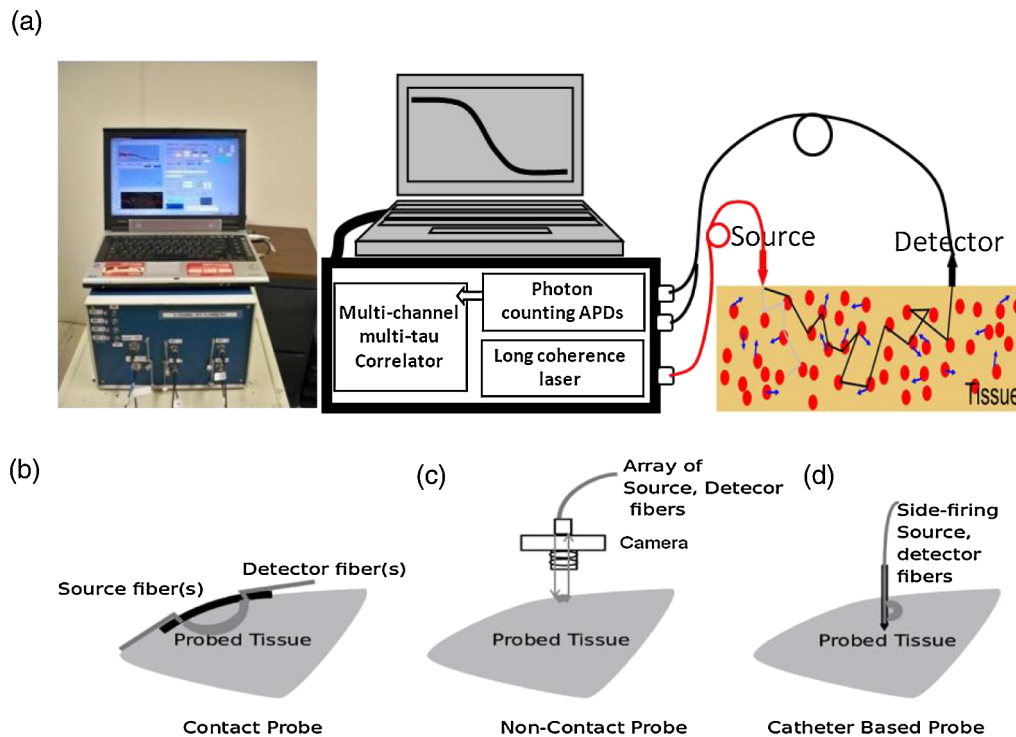

Fig. 1 (a) Portable 4-detection-channel DCS system (dimensions: $8'' \times 12'' \times 18''$), from left to right: instrument photo, DCS diagram, probe-tissue interface. Three examples of DCS probes: (b) contact probe, (c) noncontact probe, and (d) catheter-based probe.
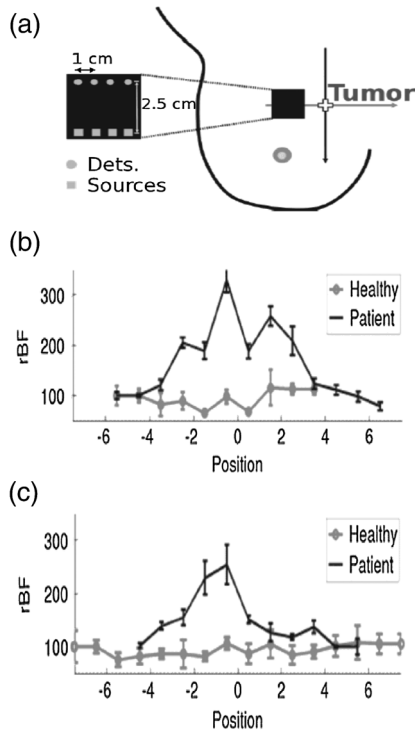
Fig. 2 (a) Handheld probe with four source-detector pairs is scanned horizontally and vertically in 1-cm increments spanning the estimated tumor region as well as the surrounding healthy tissue. Representative rBF scans from one patient with a malignant tumor and a healthy volunteer are shown for both (b) horizontal and (c) vertical scans. Probe position is indicated relative to expected tumor center (position 0). Courtesy of T. Durduran.[25]

over the tumor. Consequently, the flow contrast observed was attributable to the tumor and not the natural heterogeneity of the healthy breast. Patients can be categorized into three groups based on tumor blood flow measurements: (1) a group with very little flow heterogeneity, i.e., healthy breasts (2.7% variation, $n = 2$); (2) a group wherein the flow increased up to 230% of that of healthy tissue, i.e., malignant tumors ($n = 2$); and (3) a group wherein a moderate flow increase up to 153% was observed, i.e., benign tumors ($n = 3$). These results were in qualitative agreement with previous Doppler ultrasound and PET[60–65] results where ~470 550% increases in blood flow were reported in malignant tumors with smaller contrasts in benign cases.[63] It is clearly demonstrated from the findings above that robust flow contrasts in palpable tumors can be detected by DCS. In a separate study, breast tumor-to-normal contrasts in blood flow, oxygenation, and metabolism ($TMRO_2$) have also been observed.[28]

4 Therapeutic Applications

Various cancer therapies in animals and humans have been evaluated using DCS/NIRS instruments, including antivascular therapy/PDT in murine tumors[5,35,52,55–57] and chemoradiotherapy/PDT in human tumors.[26–29,53]

4.1 Tumor Blood Flow Provides Early Prediction of Long-term PDT Efficacy

A DCS system (see Fig. 1(a)) and a noncontact camera probe [see Figs. 1(c) and 3(a)] were used to monitor the relative blood

flow (rBF) of murine tumors ($n = 15$) during illumination for Photofrin-PDT and at specific time points after treatment.[5] Figure 3(b) shows the typical tumor rBF changes during PDT from one mouse. Within minutes of beginning PDT, rBF rapidly increased, followed by a decline and subsequent peaks and declines. Although intersubject variations in tumor blood flow responses existed, PDT induced a similar antivascular effect (i.e., blood flow reduction) in all murine tumors. The slope (flow reduction rate) and duration (interval time, data not shown) over which rBF decreased following the initial PDT-induced increase was highly associated with treatment durability [see Fig. 3(c)]. The treatment durability was measured as the time of tumor growth to a volume of 400 mm^3 from a pretreatment baseline of 100 mm^3. These findings were consistent with the hypothesis that treatment efficacy is a function of tumor oxygenation during PDT; under oxygen-limited conditions (i.e., rapidly declining blood flow), treatment efficacy was abrogated. After PDT, all animals showed decreases in rBF at 3 hours and
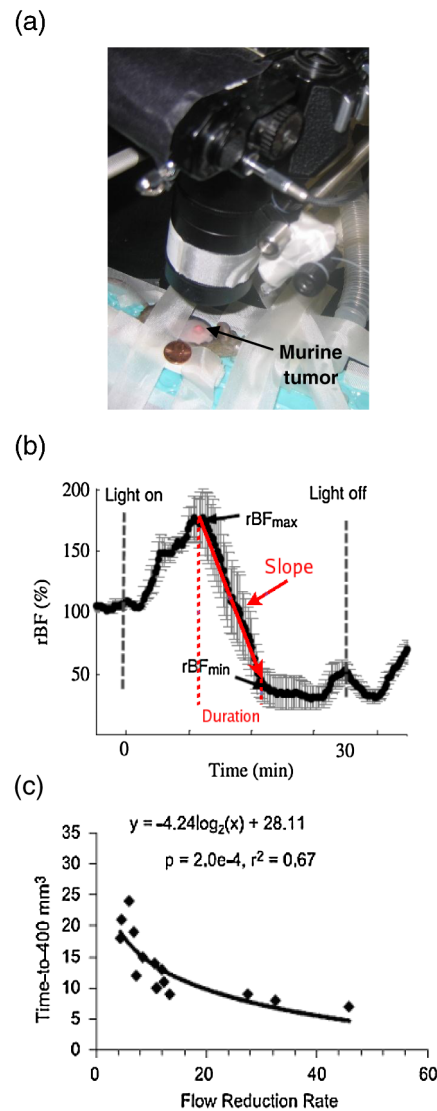

Fig. 3 (a) Photo of noncontact camera probe, (b) representative trace of tumor blood flow (rBF) during PDT, and (c) correlation between treatment durability (time-to-400 mm^3) and flow reduction rate (slope) during PDT.[5]

6 hours, and rBF at these time points was also predictive of tumor response (data not shown).[5]

These results demonstrate that DCS-measured changes in tumor rBF during and after Photofrin-PDT are predictive of treatment efficacy and suggest that real-time blood flow monitoring may be useful for treatment planning.

4.2 Monitoring of Human Prostate during PDT

Armed with promising results from the murine models above, Yu et al.[28] proceeded to adapt the DCS system for use in a Phase I clinical trial of interstitial human prostate PDT. A thin side-illumination fiber-optic probe [see Figs. 1(d) and 4(a)] containing source and detector fibers was constructed with multiple source-detector separations (0.5 to 1.5 cm).[28] The fiber-optic probe was placed inside an 18-gauge catheter (inner diameter <1 mm) that had already been inserted into the center of patient's prostate gland. Five patients with locally recurrent prostate cancer in motexafin lutetium (MLu)-mediated PDT were measured. The prostate was illuminated sequentially in several quadrants (e.g., Q1 to Q4) until the entire gland was treated. Measured rBF variation showed a similar trend in each individual.

Figures 4(b) and 4(c) show typical rBF responses over the courses of PDT in two prostatic tumors. As was the case for murine tumors,[5] a sharp decrease in prostate rBF was observed ($-41 \pm 12\%$, $n = 5$), suggesting an antivascular effect by PDT.
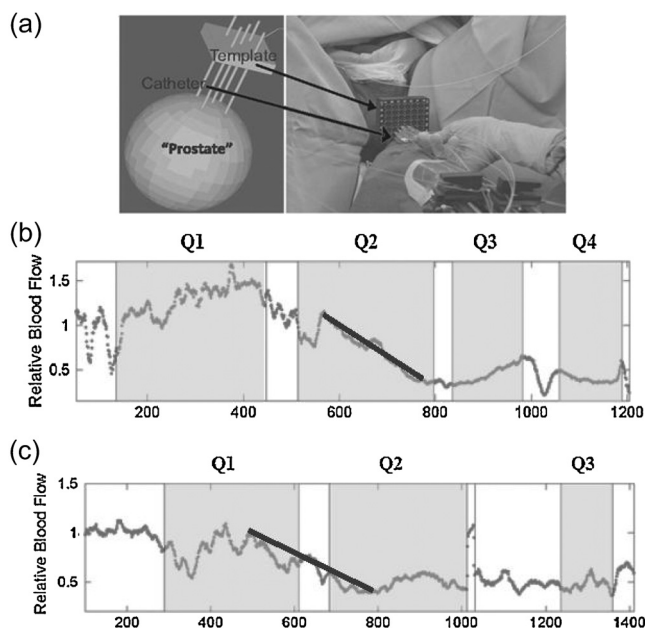

Fig. 4 (a) Custom-made template for guidance of placing catheters for prostate PDT. The treatment light was administered through the cylindrical diffusing fibers inside the thin catheters. The small side-illuminated probe was placed in the center of the prostate before PDT through one of the catheters. The catheter remained in place throughout PDT; (b) and (c) Tumor blood flow responses during PDT as a function of time measured from two prostates. Pretreatment flow value was defined as "1" (100%) in all patients. Multiple quadrants of the prostates (e.g., Q1 to Q4) were illuminated sequentially until the entire gland was treated. The illumination periods are presented as shaded areas. Flow reduction rate is defined by the slope of the decrease in blood flow. This figure is reproduced from Figs. 1 and 3 in Ref. 28.

The flow reduction rate (slope) during PDT showed large interprostate heterogeneities: 15%/min in Fig. 4(b) versus 10%/min in Fig. 4(c). On average ($n = 5$), the flow reduction rate from the five subjects was $12 \pm 5\%$/min.

Even though this study made no attempts to correlate clinical outcomes with DCS-measured flow responses during PDT, it is clear that PDT-induced flow responses hold potential for the prediction of treatment outcomes in humans, as shown in murine tumor models.

4.3 Monitoring of Head and Neck Tumor Undergoing Radiotherapy

Researchers have also explored the potential of DCS/NIRS for monitoring early rBF, tissue oxygen saturation (StO_2), and total hemoglobin concentration (THC) responses to radiotherapy in patients with head and neck tumors.[29] The rBF, StO_2, and THC in superficial neck tumor nodes of patients were measured before and throughout the radiation therapy period.

The protocol for this experiment consisted of preradiation measurements as baseline data, followed by weekly measurements for each individual until the treatment was completed. Each patient received daily fractionated radiation over 6.4 weeks and the optical measurements were completed just before treatment began each week. To obtain DCS/NIRS measurements a handheld probe was placed on the neck tumor [see Figs. 1(b) and 5(a)] and the forearm muscle (for control purposes) respectively. The largest source-detector separation of the probe was 3 cm for both optical techniques. Tumor-to-normal hemodynamic contrast was obtained by normalizing the tumor data to the arm muscle data.

The left panel of Fig. 5 shows the changes of rBF (b), StO_2 (c), and THC (d) averaged over seven patients who have complete responses (based on the tumor volume changes after treatment) to radiation therapy. Different patterns were exhibited from different individuals for the weekly rBF, StO_2, and THC kinetics, including significant early blood flow changes during the first two weeks. Average rBF increased ($52.7 \pm 9.7\%$) in the first week and decreased ($42.4 \pm 7.0\%$) in the second week. Average StO_2 increased from the baseline value of $62.9 \pm 3.4\%$ to $70.4 \pm 3.2\%$ at the end of the second week, and average THC showed a continuous decrease from the pretreatment value of 80.7 ± 7.0 μM to 73.3 ± 8.3 μM at the end of the second week and to 63.0 ± 8.1 μM at the end of the fourth week of therapy.

The right panel of Fig. 5 demonstrates the changes of rBF (e), StO_2 (f), and THC (g) observed from a partial responder. This patient exhibited substantially different tumor hemodynamic response during the therapy compared to the seven complete responders (see the left panel in Fig. 5); in this case rBF exhibited a continual increase, while StO_2 and THC also tended to increase over the course of treatment. For this patient, pretherapy CT showed a large necrotic nodal mass, and the tumor was still relatively large and palpable at the end of the therapy. Post-surgical pathology confirmed the existence of residual tumor, and so the patient was considered to be a partial responder.

This study demonstrates the potential value of diffuse optical measurements for early prediction of cancer treatment outcomes (e.g., complete responders versus partial responders) in clinic.
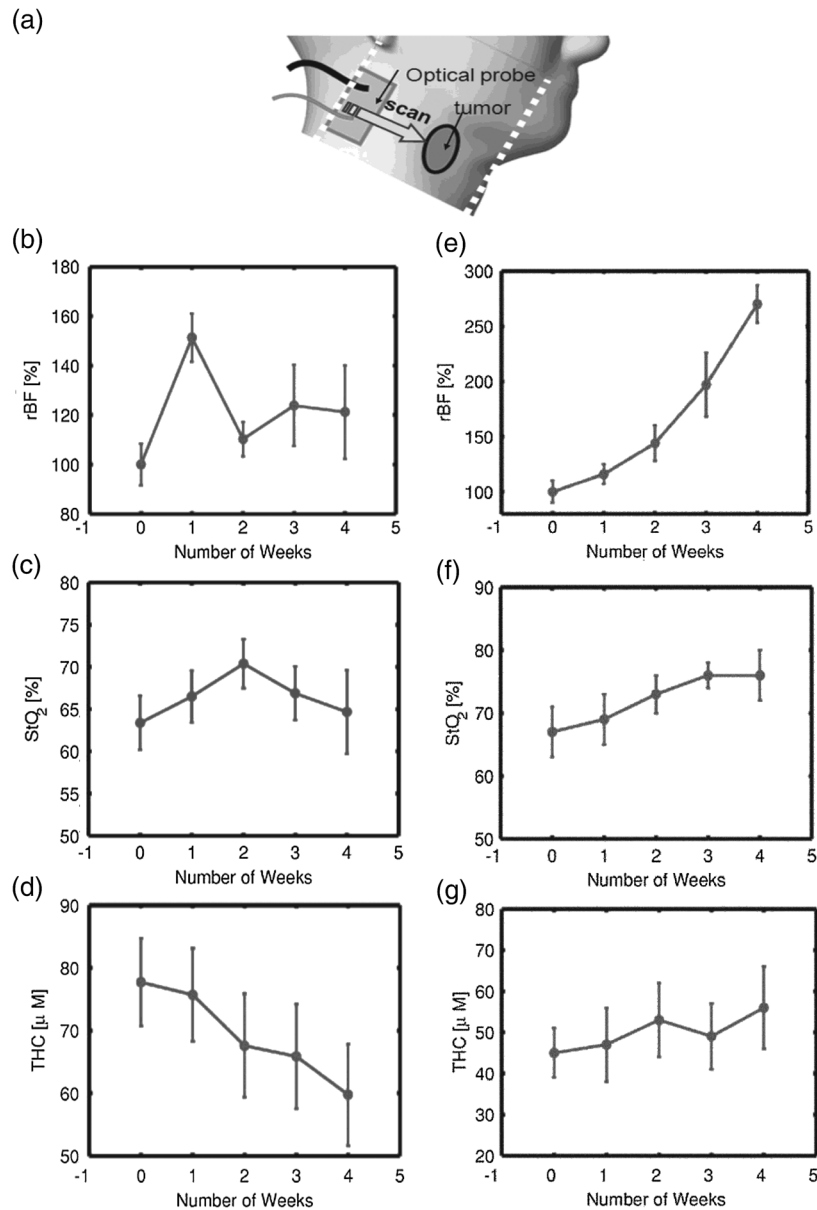
Fig. 5 (a) Handheld probe for scanning the head/neck tumor. (b) Average tumor rBF changes during radiotherapy averaged over seven patients who were complete responders to radiation treatment. (c) Average tumor blood oxygen saturation (StO_2). (d) Average tumor THC. (e) rBF observed from a partial responder. (f) StO_2 from a partial responder (g) THC from a partial responder. Courtesy of U. Sunar.[29]

5 Discussion and Conclusions

DCS is a novel technology which allows for noninvasive and continuous measurement of blood flow in relatively deep (several centimeters) tumors before, during, and after cancer therapies. During the past decade, this technique has been adopted by several research groups from its theoretical conception to multiple cancer studies in animals and humans. DCS measurements show promise for differentiating tumors from healthy tissues and benign from malignant tumors, and demonstrate potential for early prediction of individual treatment outcomes. The hybrid optical approach combining DCS and NIRS provides different types of functional parameters (i.e., blood flow, blood oxygenation, tumor oxygen metabolism) which may have different sensitivity in detection of cancers and treatment responses.

Clinical noninvasive investigations of hemodynamic responses in various tumors (e.g., breast, head and neck, prostate) during various therapies (e.g., chemotherapy, radiation therapy, photodynamic therapy) using DCS/NIRS have been demonstrated in multiple pilot human studies. The results from these clinical studies show that tumors exhibited significant hemodynamic changes in the first several days or weeks of treatment and even during therapy delivery. Such information may be useful for the prediction and optimization of cancer therapy in a time-sensitive fashion. These early and continuous changes can be easily detected by optical technologies that have various important advantages over one-time fMRI, CT, or PET in terms of being noninvasive, fast, portable, inexpensive, and continuous. No significant risks to patient populations are associated with these optical measurements.

However, it should be noticed that most of the clinical studies reported so far are feasibility studies in small patient populations, and tumor hemodynamic responses to therapy have been monitored only for short periods (up to several weeks). Longitudinal studies in large patient populations are needed to translate the techniques to clinic for routine monitoring and management of cancers and therapies.

Some theoretical/technical issues exist when applying DCS to biological tissues. For example, a quantitative microscopic explanation about why the Brownian-motion model fits the autocorrelation curves more effectively than the random ballistic flow model is still sought by researchers in the field. In a recently published paper, Carp et al.[66] commented that the random ballistic flow model assumes successive scattering events occur on scattering centers with uncorrelated velocity vectors. This assumption is valid if the probability of having two or more scattering events in a single blood vessel is low. However, photons entering any blood vessel larger than a capillary most likely undergo multiple scattering before exiting. Therefore, the random ballistic flow assumption can be invalidated considering that the majority of blood volume is contained in such larger vessels.[67] While the simplified Brownian-motion model appears to work well, it assumes that the ballistic to random-walk hydrodynamic transition in the RBC diffusion occurs at time scales shorter than those probed by DCS measurements. Since there is no data to support this assumption, Carp et al. proposed a hydrodynamic diffusion model that includes both ballistic flow at short delay time and diffusive motion at later delay time to provide the best fit for the experimental data.[66] This approach is promising, but it remains desirable to carry out more experiments in order to generate fundamental understanding of the origins of the DCS blood flow index.

Moreover, the advent of DCS technology has brought the need to further investigate its potential errors, notably the assumption of constant optical properties (μ_a and μ_s') and approximation of the biological tissues as an ergodic system. The flow index produced by DCS measurement is based on a solution to the correlation diffusion equation (see Eq. 2) which includes parameters of μ_a and μ_s'. A recent study using tissue phantoms has shown that inaccurate μ_s' assumptions resulted in much greater flow index errors than inaccurate μ_a.[21] Examination of a clinical study involving human head and neck tumors indicates up to 280% flow index errors resulted from interpatient optical property variations. These findings suggest that studies involving significant μ_a and μ_s' changes should concurrently measure flow index and optical properties for accurate extraction of blood flow information. Another potential error comes from the approximation of measured biological tissues as an ergodic system. The Siegert relation (see Eq. 1) does not apply to nonergodic systems. i.e., the time-averaged measurements are not equivalent to the ensemble-average computed by the various photon correlation spectroscopy theories.[58] Ultimately, the field has moved forward because previous validation studies have shown that DCS flow measurements agree with other microvasculature flow measurement techniques, suggesting such potential errors may not be significant. However, biological tissues are not ergodic, since they have both static (e.g., nuclei, mitochondria) and dynamic (moving RBCs) scattering components. An ensemble averaging technique has been proposed to obtain the proper correlation function.[58] Basically, the idea is to move the sample (or the source and detector) during the integration of a correlation function. In this way, an ensemble of static components is measured and thus the desired ensemble average of the speckles' intensity can be obtained. This method, however, has not been applied in clinic mainly due to the difficulty of moving biological samples. Interestingly, in a few test cases, comparison between the standard measurement scheme and the moving sample has been carried out in vivo; differences between the two approaches were small, perhaps because the static components were small in practice. Further investigations are needed to evaluate the errors generated by the ergodic approximation for the nonergodic biological system.

Although much work remains to be done, it is expected that with further technology developments and more clinical exploration, DCS will emerge as one of the choices for clinical investigation of cancers and treatment responses.

References

1. J. Niederhuber, "Progress -reports 4th-report," http://edrn.nci.nih.gov/docs/progress-reports/edrn_4th-report_200801.pdf (2008).
2. V. R. Kondepati, H. M. Heise, and J. Backhaus, "Recent applications of near-infrared spectroscopy in cancer diagnosis and therapy," *Anal. Bioanal. Chem.* **390**(1), 125–139 (2008).
3. H. W. Wang et al., "Treatment-induced changes in tumor oxygenation predict photodynamic therapy outcome," *Cancer Res.* **64**(20), 7553–7561 (2004).
4. D. J. Carlson, "Mechanism of intrinsic radiation sensitivity: the effects of DNA damage repair, oxygen, and radiation quality," PhD Dissertation., Purdue University, West Lafayette (2006).
5. G. Yu et al., "Noninvasive monitoring of murine tumor blood flow during and after photodynamic therapy provides early assessment of therapeutic efficacy," *Clin. Cancer Res.* **11**(9), 3543–3552 (2005).
6. M. E. Van Dort, A. Rehemtulla, and B. D. Ross, "PET and SPECT imaging of tumor biology: new approaches towards oncology drug discovery and development," *Curr. Comput. Aided Drug Des.* **4**(1), 46–53 (2008).
7. B. W. Pogue et al., "Breast tissue and tumor hemoglobin and oxygen saturation imaging with multi-spectral near infrared computed tomography," in *Advances in Experimental Medicine and Biology Series*, Plenum Press, New York (2001).
8. V. Ntziachristos et al., "MRI-guided diffuse optical spectroscopy of malignant and benign breast lesions," *Neoplasia* **4**(4) 347–354 (2002).
9. S. Fantini et al., "Assessment of the size, position, and optical properties of breast tumors in vivo by noninvasive optical methods," *Appl. Opt.* **37**(10), 1982–1989 (1998).
10. Q. Zhu, S. Tannenbaum, and S. H. Kurtzman, "Optical tomography with ultrasound localization for breast cancer diagnosis and treatment monitoring," *Surg. Oncol. Clin. N. Am* **16**(2), 307–321 (2007).
11. Q. Fang et al., "Combined optical and X-ray tomosynthesis breast imaging," *Radiology* **258**(1), 89–97 (2011).

12. B. J. Tromberg et al., "Assessing the future of diffuse optical imaging technologies for breast cancer management," *Med. Phys.* **35**(6), 2443–2451 (2008).

13. H. Jiang, S. Ramesh, and M. Bartlett, "Combined optical and fluorescence imaging for breast cancer detection and diagnosis," *Crit. Rev. Biomed. Eng.* **28**(3–4), 371–375 (2000).

14. H. Liu et al., "Near-infrared spectroscopy and imaging of tumor vascular oxygenation," *Methods Enzymol.* **386**, 349–378 (2004).

15. R. Choe et al., "Differentiation of benign and malignant breast tumors by in-vivo three-dimensional parallel-plate diffuse optical tomography," *J. Biomed. Opt.* **14**(2), 024020 (2009).

16. D. A. Boas and A. G. Yodh, "Spatially varying dynamical properties of turbid media probed with diffusing temporal light correlation," *J. Opt. Soc. Am. A: Opt. Image Sci. Vis.* **14**(1), 192–215 (1997).

17. D. A. Boas, L. E. Campbell, and A. G. Yodh, "Scattering and imaging with diffusing temporal field correlations," *Phys. Rev. Lett.* **75**(9), 1855–1858 (1995).

18. D. J. Pine et al., "Diffusing-wave spectroscopy," *Phys. Rev. Lett.* **60**, 1134–1137 (1988).

19. G. Maret and P. E. Wolf, "Multiple light scattering from disordered media. The effect of brownian motion of scatterers," *Z. Phys. B* **65**, 409–413 (1987).

20. J. Li et al., "Noninvasive detection of functional brain activity with near-infrared diffusing-wave spectroscopy," *J. Biomed. Opt.* **10**(4), 044002 (2005).

21. D. Irwin et al., "Influences of tissue absorption and scattering on diffuse correlation spectroscopy blood flow measurements," *Biomed. Opt. Express* **2**(7), 1969–1985 (2011).

22. M. Belau et al., "Noninvasive observation of skeletal muscle contraction using near-infrared time-resolved reflectance and diffusing-wave spectroscopy," *J. Biomed. Opt.* **15**(5), 057007 (2010).

23. Y. Shang et al., "Portable optical tissue flow oximeter based on diffuse correlation spectroscopy," *Opt. Lett.* **34**(22), 3556–3558 (2009).

24. G. Dietsche et al., "Fiber-based multispeckle detection for time-resolved diffusing-wave spectroscopy: characterization and application to blood flow detection in deep tissue," *Appl. Opt.* **46**(35), 8506–8514 (2007).

25. T. Durduran et al., "Diffuse optical measurement of blood flow in breast tumors," *Opt. Lett.* **30**(21), 2915–2917 (2005).

26. G. Yu et al., "Time-dependent blood flow and oxygenation in human skeletal muscles measured with noninvasive near-infrared diffuse optical spectroscopies," *J. Biomed. Opt.* **10**(2), 024027 (2005).

27. T. Durduran et al., "Diffuse optical measurement of blood flow, blood oxygenation, and metabolism in a human brain during sensorimotor cortex activation," *Opt. Lett.* **29**(15), 1766–1768 (2004).

28. G. Yu et al., "Real-time in situ monitoring of human prostate photodynamic therapy with diffuse light," *Photochem. Photobiol.* **82**(5), 1279–1284 (2006).

29. U. Sunar et al., "Noninvasive diffuse optical measurement of blood flow and blood oxygenation for monitoring radiation therapy in patients with head and neck tumors: a pilot study," *J. Biomed. Opt.* **11**(6), 064021 (2006).

30. C. Zhou et al., "Diffuse optical monitoring of blood flow and oxygenation in human breast cancer during early stages of neoadjuvant chemotherapy," *J. Biomed. Opt.* **12**(5), 051903 (2007).

31. G. Yu et al., "Intraoperative evaluation of revascularization effect on ischemic muscle hemodynamics using near-infrared diffuse optical spectroscopies," *J. Biomed. Opt.* **16**(2), 027004 (2011).

32. Y. Shang et al., "Cerebral monitoring during carotid endarterectomy using near-infrared diffuse optical spectroscopies and electroencephalogram," *Phys. Med. Biol.* **56**(10), 3015–3032 (2011).

33. T. Durduran et al., "Transcranial optical monitoring of cerebrovascular hemodynamics in acute stroke patients," *Opt. Express* **17**(5), 3884–3902 (2009).

34. N. Roche-Labarbe et al., "Noninvasive optical measures of CBV, StO (2), CBF index, and rCMRO(2) in human premature neonates' brains in the first six weeks of life," *Hum. Brain Mapp.* **31**(3), 341–352 (2010).

35. C. Menon et al., "An integrated clinically relevant approach to measuring tumor oxygen status using VEGF-transfected human melanoma xenografts as a model," *Cancer Res.* **63**, 7232–7240 (2003).

36. R. C. Mesquita et al., "Hemodynamic and metabolic diffuse optical monitoring in a mouse model of hindlimb ischemia," *Biomed. Opt. Express* **1**(4), 1173–1187 (2010).

37. M. N. Kim et al., "Noninvasive measurement of cerebral blood flow and blood oxygenation using near-infrared and diffuse correlation spectroscopies in critically brain-injured adults," *Neurocrit. Care* **12**(2), 173–180 (2010).

38. E. M. Buckley et al., "Cerebral hemodynamics in preterm infants during positional intervention measured with diffuse correlation spectroscopy and transcranial Doppler ultrasound," *Opt. Express* **17**(15), 12571–12581 (2009).

39. C. Zhou et al., "Diffuse optical monitoring of hemodynamic changes in piglet brain with closed head injury," *J. Biomed. Opt.* **14**(3), 034015 (2009).

40. G. Yu et al., "Validation of diffuse correlation spectroscopy for muscle blood flow with concurrent arterial spin labeled perfusion MRI," *Opt. Express* **15**(3), 1064–1075 (2007).

41. J. Li et al., "Transient functional blood flow change in the human brain measured noninvasively by diffusing-wave spectroscopy," *Opt. Lett.* **33**(19), 2233–2235 (2008).

42. J. P. Culver et al., "Diffuse optical tomography of cerebral blood flow, oxygenation, and metabolism in rat during focal ischemia," *J. Cereb. Blood Flow Metab.* **23**(8), 911–924 (2003).

43. C. Cheung et al., "In vivo cerebrovascular measurement combining diffuse near-infrared absorption and correlation spectroscopies," *Phys. Med. Biol.* **46**(8), 2053–2065 (2001).

44. J. P. Culver et al., "Diffuse optical measurement of hemoglobin and cerebral blood flow in rat brain during hypercapnia, hypoxia and cardiac arrest," in Adv. Exp. Biol., in *Oxygen Transport to Tissue*, D. F. Wilson, S. M. Evans, J. Biaglow, and A. Pastuszko, eds., Plenum Press, New York, pp. 293–298 (2002).

45. C. Zhou et al., "Diffuse optical correlation tomography of cerebral blood flow during cortical spreading depression in rat brain," *Opt. Express* **14**, 1125–1144, (2006).

46. L. Gagnon et al., "Investigation of diffuse correlation spectroscopy in multi-layered media including the human head," *Opt. Express* **16**(20), 15514–15530 (2008).

47. T. Durduran et al., "Optical measurement of cerebral hemodynamics and oxygen metabolism in neonates with congenital heart defects," *J. Biomed. Opt.* **15**(3), 037004 (2010).

48. B. L. Edlow et al., "The effects of healthy aging on cerebral hemodynamic responses to posture change," *Physiol. Meas.* **31**(4), 477–495 (2010).

49. M. Diop et al., "Calibration of diffuse correlation spectroscopy with a time-resolved near-infrared technique to yield absolute cerebral blood flow measurements," *Biomed. Opt. Express* **2**(7), 2068–2081 (2011).

50. Y. Shang et al., "Effects of muscle fiber motion on diffuse correlation spectroscopy blood flow measurements during exercise," *Biomed. Opt. Express* **1**(2), 500–511 (2010).

51. K. L. Du et al., "Preliminary results of interstitial motexafin lutetium-mediated PDT for prostate cancer," *Lasers Surg. Med.* **38**(5), 427–434 (2006).

52. U. Sunar et al., "Hemodynamic responses to antivascular therapy and ionizing radiation assessed by diffuse optical spectroscopies," *Opt. Express* **15**(23), 15507–15516 (2007).

53. U. Sunar et al., "Monitoring photobleaching and hemodynamic responses to HPPH-mediated photodynamic therapy of head and neck cancer: a case report," *Opt. Express* **18**(14), 14969–14978 (2010).

54. T. L. Becker et al., "Monitoring blood flow responses during topical ALA-PDT," *Biomed. Opt. Express* **2**(1), 123–130 (2010).

55. T. M. Busch et al., "Increasing damage to tumor blood vessels during motexafin lutetium-PDT through use of low fluence rate," *Radiat Res.* **174**(3), 331–340 (2010).

56. T. M. Busch et al., "Fluence rate-dependent intratumor heterogeneity in physiologic and cytotoxic responses to Photofrin photodynamic therapy," *Photochem. Photobiol. Sci.* **8**(12), 1683–1693 (2009).

57. A. Marrero et al., "Aminolevulinic acid-photodynamic therapy combined with topically applied vascular disrupting agent vadimezan leads to enhanced antitumor responses," *Photochem. Photobiol.* **87**(4), 910–919 (2011).

58. D. Boas, "Diffuse photon probes of structural and dynamical properties of turbid media: theory and biomedical applications," PhD Dissertation, University of Pennsylvania (1996).

59. S. O. Rice, "Mathematical analysis of random noise," in *Noise and Stochastic Processes*, N. Wax, ed., Dover, New York, p. 133 (1954).

60. R. P. Beaney et al., "Positron emission tomography for in-vivo measurement of regional blood flow, oxygen utilisation, and blood volume in patients with breast carcinoma," *Lancet* **1**(8369), 131–134 (1984).
61. C. B. Wilson et al., "Quantitative measurement of monoclonal antibody distribution and blood flow using positron emission tomography and 124iodine in patients with breast cancer," *Int. J. Cancer* **47**(3), 344–347 (1991).
62. C. B. Wilson et al., "Measurements of blood flow and exchanging water space in breast tumors using positron emission tomography: a rapid and noninvasive dynamic method," *Cancer Res.* **52**(6), 1592–1597 (1992).
63. H. Madjar et al., "Color Doppler and duplex flow analysis for classification of breast lesions," *Gynecol. Oncol.* **64**(3), 392–403 (1997).
64. D. O. Cosgrove et al., "Color Doppler signals from breast tumors. Work in progress," *Radiology* **176**(1), 175–180 (1990).
65. R. P. Kedar et al., "Breast carcinoma: measurement of tumor response to primary medical therapy with color Doppler flow imaging," *Radiology* **190**(3), 825–830 (1994).
66. A. S. Carp et al., "Due to intravascular multiple sequential scattering, diffuse correlation spectroscopy of tissue primarily measures relative red blood cell motion within vessels," *Biomed. Opt. Express* **2**(7), 2047–2054 (2011).
67. T. Q. Duong and S. G. Kim, "In vivo MR measurements of regional arterial and venous blood volume fractions in intact rat brain," *Magn. Reson. Med. Sci.* **43**(3), 393–402 (2000).